Maximum-Likelihood Estimation of Circle Parameters Via Convolution

Emanuel E. Zelniker, *Student Member, IEEE,* and I. Vaughan L. Clarkson, *Senior Member, IEEE*

***Abstract*—The accurate fitting of a circle to noisy measurements of circumferential points is a much studied problem in the literature. In this paper, we present an interpretation of the maximum-likelihood estimator (MLE) and the Delogne–Kåsa estimator (DKE) for circle-center and radius estimation in terms of convolution on an image which is ideal in a certain sense. We use our convolution-based MLE approach to find good estimates for the parameters of a circle in digital images. In digital images, it is then possible to treat these estimates as preliminary estimates into various other numerical techniques which further refine them to achieve subpixel accuracy. We also investigate the relationship between the convolution of an ideal image with a "phase-coded kernel" (PCK) and the MLE. This is related to the "phase-coded annulus" which was introduced by Atherton and Kerbyson who proposed it as one of a number of new convolution kernels for estimating circle center and radius. We show that the PCK is an approximate MLE (AMLE). We compare our AMLE method to the MLE and the DKE as well as the Cramér–Rao Lower Bound in ideal images and in both real and synthetic digital images.**

***Index Terms*—Circle fitting, convolution, Cramér–Rao lower bound (CRLB), least squares, maximum-likelihood estimation (MLE).**

I. Introduction

THE accurate fitting of a circle to noisy measurements of points on its circumference is an important and much-studied problem in statistics. It often arises in digital image processing when circular features in digital images are sought. The reasons for this range from quality inspection for mechanical parts [1] to fitting circles for particle trajectories [2], [3]. Circle fitting also has applications in archaeology [4], microwave engineering [5], and ball detection in robotic vision systems [6].

In the literature, we can identify two basic approaches for fitting circles. One approach is from a statistical point of view [1], [7], [8], where the noisy circle points are treated as a list of measurements; usually real-valued coordinates. The other is an image based approach such as the circular Hough transform (CHT) [9], [10] and the phase-coded annulus (PCA) [11], [12].

The first detailed statistical analysis to be published appears to be that of Chan [13]. He proposes a "circular functional relationship," which we also use as the basis for our investigations. In this model, it is assumed that the measurement errors are instances of independent and identically distributed (i.i.d.) random variables. Additionally, the points are assumed to lie at fixed but unknown angles around the circumference, i.e., not only are the center and radius of the circle unknown parameters to be estimated, but so are the angles of each circumferential point. He derives a method to find the maximum-likelihood estimator (MLE) when the errors have a Gaussian distribution. This method is identical to the least-squares method of [14]. He also examines the consistency of the estimator.

Chan and Thomas [15] have investigated the Cramér–Rao lower bound (CRLB) for estimation in the circular functional model, but see also [16].

A disadvantage of the MLE is that it can be difficult to analyze. From a numerical point of view, another disadvantage is that the only known algorithms for computing the MLE are iterative. Furthermore, there are instances in which there is no minimum, but rather a stationary point, or several local minima in the likelihood function [8], [17]. The difficulties with the MLE were recognized by Kåsa [5], who proposes using a simple estimator due to Delogne [18] which is relatively easy to analyze and also to compute. This estimator has subsequently been independently rediscovered at least four times [19]–[22].

Berman and Culpin [17] have carried out a detailed statistical analysis of both the MLE and the Delogne–Kåsa estimator (DKE). Specifically, they prove some results regarding the asymptotic consistency and variance of the estimates. Zelniker and Clarkson [23], [24] examine the properties of the DKE for fixed (small) sample sizes rather than its asymptotic properties.

Because of the analytical difficulties which are associated with the MLE for circles, there have been a number of iterative algorithms proposed which calculate the MLE numerically. Typically, these are based on gradient ascent over the (log) likelihood function. The Newton–Raphson (NR) algorithm is an obvious choice but is well known to have a propensity to get stuck in local minima, diverge to infinity, or enter a limit cycle. This can be because of the nature of the objective function or the incorrect or unfortunate choice of starting point. In the case of circle fitting, it has been shown that NR can easily fail [8], [17]. For this reason, there have been several techniques proposed to circumvent the convergence difficulties of NR.

Späth [7] provides a descent algorithm for circle fitting. A numerical algorithm is proposes for the MLE which uses two types of iterating steps, by partitioning the set of parameters. The algorithm is initialized from a point which is evaluated using the DKE. Späth's algorithm is not guaranteed to converge, but it does have the desirable property that the likelihood of its estimate is nondecreasing from iteration to iteration. Chernov and Lesort [8] propose another algorithm to minimize the objective

Manuscript received July 22, 2004; revised January 6, 2005. E. E. Zelniker was supported by a scholarship from the Commonwealth Scientific and Industrial Research Organization. Preliminary versions of portions of this paper were presented at DICTA 2003 and EUSIPCO 2004. The associate editor coordinating the review of this manuscript and approving it for publication was Dr. Ivan W. Selesnick.

The authors are with the School of Information Technology and Electrical Engineering, University of Queensland Queensland, 4072, Australia.

Digital Object Identifier 10.1109/TIP.2005.863965

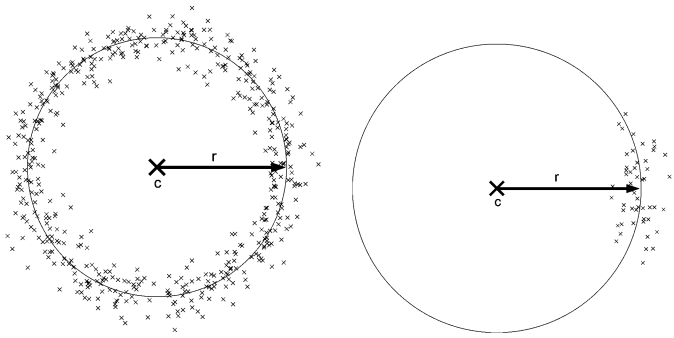

Fig. 1. Two examples of noisy measurements of points on the circumference of a circular arc.

function in [7] which has less chance of diverging and a faster rate of convergence than the previous mentioned algorithms, however each iteration is more computationally intensive.

As well as the statistical approach to circle parameter estimation, another setting for circle fitting is to be found in image analysis. Here, an image of a scene is analyzed to determine the center and radius of a circular object. Computation is performed on intensities and pixels rather than on a list of individually detected circumferential points. The CHT is an iterative approach to circle parameter estimation in digital images in the sense that it has to be evaluated for each size of circle (normally in a predetermined range). A three-dimensional (3-D) Hough accumulator space is chosen where every point in this space represents a circle of a certain size in x–y space. The Hough space can be viewed as an intensity space and the coordinate with the highest intensity corresponds to the circle estimates. Computation of the CHT is relatively slow and memory intensive. As a result, there has been some interest in developing algorithms that achieve similar or better performance in detection and estimation of circles in images while using less computational and memory resources. Atherton and Kerbyson [11], [12] state that the Hough transform can be implemented by convolving a single circle with an edge magnitude image (matched filtering). They build on this idea by defining an orientation annulus which detects a range of radii of circles, but also uses edge orientation information by taking the dot-product between the image edge orientation and an orientation field within the annulus. A complex PCA is also described which detects a range of radii of circles by using phase to code for radius. The complex vector convolution of this annulus with an edge magnitude image results in a circle detection operation which estimates both the center and radius of the circle.

The central theme of this paper is to show the overlap between the statistical viewpoint and the image-based viewpoint. We show that it is possible to exactly implement the MLE as well as the DKE in terms of convolution under a certain model for an ideal image. In our model, an ideal image is an unbounded image with continuous values in intensity and in spatial coordinates. The measurements of the statistical model are represented as delta functions within the image model. Although an exact correspondence between the statistical model and our image model holds for ideal images, we find that our technique can also be adapted to digital images to produce coarser estimates, i.e., within one pixel. However, these can be used as a starting point for one of the numerical optimization methods if subpixel accuracy is required.

We also show that an approximate MLE (AMLE) can be developed for these same ideal images. We show how our AMLE can be calculated by convolution and it turns out that the convolution kernel is related to the PCA. Moreover, we show through examples that the AMLE and PCA have advantages in real-world digital images where the scene contains objects other than a single circle.

The paper is arranged as follows. In Section II, we provide a brief overview of the statistical viewpoint background, the CRLB, the MLE, and we discuss the DKE. In Section III, we present the necessary background on techniques in image processing for the detection of circles and estimation of their parameters. Section IV defines an ideal image of noisy circumferential points in order to exactly describe the MLE and DKE via convolution. In Section V, we define the objective function of the AMLE. We show the relationship between the objective function of the AMLE and the objective function of the MLE and discuss applications to real images. In Section VI, we briefly discuss the implementation of convolution via the FFT, the memory requirements of the CHT and AMLE and how to achieve subpixel accuracy. In Section VII, we present simulation results to compare the AMLE, MLE, Chernov–Lesort (CL) algorithm, and DKE to the CRLB.

II. Statistical Background

A. Chan's Circular Functional Model

In this section, we briefly present Chan's circular functional model [13]. In this model, we assume that the positions of N points on the circumference of a circle are measured. The measurement process introduces random errors so that the Cartesian coordinates $\mathbf{p}_i = (x_i, y_i)^T, i = 1, \ldots, N$ can be expressed as

$$\mathbf{p}_i = \mathbf{c} + r\mathbf{u}(\theta_i) + \boldsymbol{\xi}_i. \tag{1}$$

Here, $\mathbf{c} = (c_1, c_2)^T$ is the center of the circle, r is its radius, the $\mathbf{u}(\theta_i) = (\cos\theta_i, \sin\theta_i)^T$ are unit vectors and the $\boldsymbol{\xi}_i$ are instances of random variables representing the measurement errors. They are assumed to be zero-mean and i.i.d. In addition, we will specify that they are Gaussian with variance σ^2.

Fig. 1 shows some data with N measurements around a circle and an arc $\mathbf{p}_1, \ldots, \mathbf{p}_N$ displaced from the circumference by noise.

B. CRLB

In order to statistically analyze the MLE, we make use of the the CRLB. This provides a theoretical lower bound for the variance of unbiased estimators for a certain amount of data N and a certain level of noise σ. The likelihood function for $\mathbf{p}_1, \ldots, \mathbf{p}_N$ is as follows:

$$L(\mathbf{c}, r, \{\theta_i\} | \mathbf{p}_1, \ldots, \mathbf{p}_N) = \frac{1}{(2\pi\sigma^2)^N} \prod_{i=1}^{N} \exp\left(-\frac{\|\mathbf{p}_i - (\mathbf{c} + r\mathbf{u}(\theta_i))\|_2^2}{2\sigma^2} \right). \quad (2)$$

The CRLB (see [25]) for Chan's circular functional model with Gaussian random variables was derived by Chan and Thomas [15] (also see [16] for a more straightforward derivation). It can be shown that the variances for the estimates of $\mathbf{c}$ and r will lie along the diagonal of the upper 3×3 submatrix of the inverse of the Fisher information matrix, which amounts to taking the inverse of

$$\frac{1}{\sigma^2} \sum_{i=1}^{N} \begin{pmatrix} \cos^2\theta_i & \cos\theta_i \sin\theta_i & \cos\theta_i \\ \cos\theta_i \sin\theta_i & \sin^2\theta_i & \sin\theta_i \\ \cos\theta_i & \sin\theta_i & 1 \end{pmatrix}^{-1}. \quad (3)$$

For equally spaced points around a full circle or circular arc spanning over an angle ϕ, the lower bounds for the variances of $\hat{c}_1, \hat{c}_2$, and $\hat{r}$ can be shown to be

$$\hat{c}_1^{\mathrm{CRLB}} = \frac{2\sigma^2}{N - \Psi}, \quad \hat{c}_2^{\mathrm{CRLB}} = \frac{2\sigma^2}{N - \Xi} \quad \text{and} \quad \hat{r}^{\mathrm{CRLB}} = \frac{\sigma^2}{N - \Omega} \quad (4)$$

where

$$\Psi = \frac{2\sin^2 c\frac{\phi}{2}}{N \sin^2 \frac{\phi}{2N}} - \frac{\sin\phi}{\sin\frac{\phi}{N}}, \quad \Xi = \frac{\sin\phi}{\sin\frac{\phi}{N}} \quad \text{and} \quad \Omega = \frac{2\sin^2\frac{\phi}{2}\sin\frac{\phi}{N}}{\sin^2\frac{\phi}{2N}\left(N\sin\frac{\phi}{N} + \sin\phi\right)}.$$

C. Maximum-Likelihood Estimation

By taking the logarithm of (2) and ignoring the constant offset and scaling, both of which are functions of N and σ only, the objective function of (2) is the log-likelihood function

$$F_{\mathrm{ML}}(\mathbf{c}, r, \{\theta_i\}) = \sum_{i=1}^{N} \|\mathbf{p}_i - (\mathbf{c} + r\mathbf{u}(\theta_i))\|_2^2. \quad (5)$$

It is not very difficult to show that the values of $\hat{\theta}_i$ which minimize (5) are those for which

$$\mathbf{u}(\hat{\theta}_i) = \frac{\mathbf{p}_i - \mathbf{c}}{\|\mathbf{p}_i - \mathbf{c}\|_2}. \quad (6)$$

Substituting (6) into (5) and simplifying, we obtain

$$F_{\mathrm{ML}}(\mathbf{c}, r) = \sum_{i=1}^{N} (\|\mathbf{p}_i - \mathbf{c}\|_2 - r)^2. \quad (7)$$

Next, it can be shown that the radius estimate is the mean of the distances from each noisy point to the center, or

$$\hat{r}_{\mathrm{ML}} = \frac{1}{N} \sum_{i=1}^{N} r_i \quad (8)$$

$$r_i = \|\mathbf{p}_i - \mathbf{c}\|_2. \quad (9)$$

Finally, using (8) and substituting into (7), it is possible to express the objective function in (5) as

$$F_{\mathrm{ML}}(\mathbf{c}) = \sum_{i=1}^{N} r_i^2 - \frac{1}{N} \left\{ \sum_{i=1}^{N} r_i \right\}^2 = N\mathrm{VAR}[r_i] \quad (10)$$

where $\mathrm{VAR}[r_i]$ is the empirical variance of the r_i.

The objective function of the log-likelihood is difficult to analyze and also to compute numerically [17]. Some examples of algorithms for computing the MLE numerically can be found in [7], [8].

D. DKE

The analytical and numerical difficulties with the MLE led Kåsa [5] to propose the use of a modified objective function, originally due to Delogne [18], which we can write as

$$F_{\mathrm{DK}}(\mathbf{c}, r) = \sum_{i=1}^{N} \left(\|\mathbf{p}_i - \mathbf{c}\|_2^2 - r^2 \right)^2. \quad (11)$$

A partial derivative shows that the sum is minimized when

$$\hat{r}_{\mathrm{DK}}^2 = \frac{1}{N} \sum_{i=1}^{N} r_i^2. \quad (12)$$

Substituting (12) into (11) and simplifying results in the following expression:

$$F_{\mathrm{DK}}(\mathbf{c}) = \sum_{i=1}^{N} r_i^4 - \frac{1}{N} \left\{ \sum_{i=1}^{N} r_i^2 \right\}^2 = N\mathrm{VAR}\left[r_i^2\right]. \quad (13)$$

III. Image-Processing Background

In this section, we will briefly outline some of the existing image-analysis algorithms for circle parameter estimation in digital images.

A. CHT

The CHT [9], [10] is an iterative approach to circle parameter estimation in images in the sense that it has to be evaluated for each center and radius in a predetermined range. Since a circle is characterized by three parameters, a 3-D Hough accumulator space is chosen where every point in this space represents a circle of a certain size in x–y space.

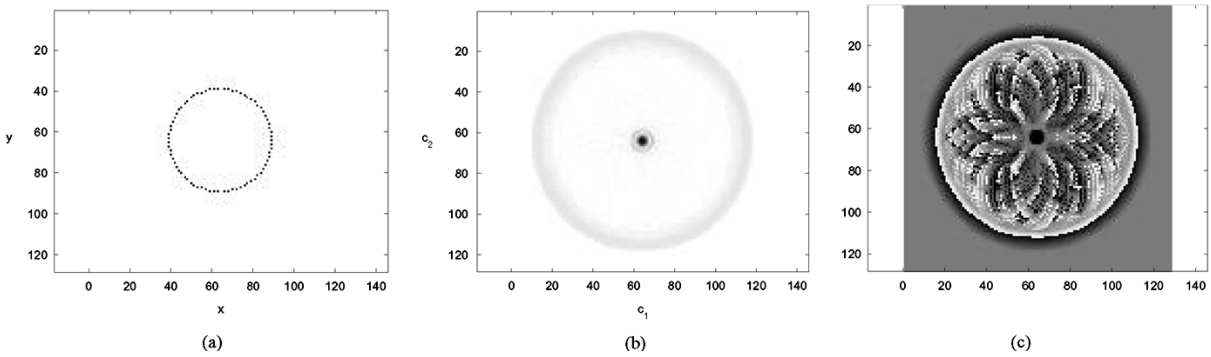

Fig. 2. Magnitude and phase of the complex convolution of the kernel in (14) with the negative of the image in Fig. 2(a). $R_{\min}$ was set to 20 and $R_{\max}$ was set to 30. (a) Negative of original image. (b) Magnitude (negative). (c) Phase (wrapped).

B. PCA

Atherton and Kerbyson [11], [12] propose a technique based on convolution. The kernel is a complex PCA that uses phase to code for a range of radii, $R_{\min}$ to $R_{\max}$

$$O_{\mathrm{PCA}}(x,y)=\begin{cases} e^{j\gamma(x,y)}, & \text{if } R_{\min}^2 < x^2+y^2 < R_{\max}^2 \\ 0, & \text{otherwise} \end{cases} \tag{14}$$

where j is the imaginary unit and $\gamma(x,y)$ is defined so that

$$\gamma(x,y)=2\pi\left(\frac{\sqrt{x^2+y^2}-R_{\min}}{R_{\max}-R_{\min}}\right). \tag{15}$$

The complex vector convolution of this annulus with an edge-magnitude image results in a circle-detection operation which uses both edge magnitude information and size information (see Fig. 2). The phase at the coordinate of the peak in the magnitude image is substituted into (15) and then it is possible to solve for the radius. In other words, if

$$F_{\mathrm{PCA}}(\mathbf{c},r)=O_{\mathrm{PCA}}(x,y)*f(x,y) \tag{16}$$

where $f(x,y)$ is an edge-magnitude image, then

$$\hat{\mathbf{c}}_{\mathrm{PCA}}=\arg\max_{(x,y)}|F_{\mathrm{PCA}}(x,y)| \tag{17}$$

$$\hat{r}_{\mathrm{PCA}}=\angle F_{\mathrm{PCA}}(\hat{\mathbf{c}}_{\mathrm{PCA}})\frac{(R_{\max}-R_{\min})}{2\pi}+R_{\min}. \tag{18}$$

C. Orientation Annulus

Another proposition of Atherton and Kerbyson [11], [12] is the *orientation annulus* (OA). It is another technique based on convolution, although the convolution is not with an edge-magnitude image but rather an edge-orientation image. The OA is designed to detect any circular object in an image whose radius is within a range of some prescribed values $R_{\min}$ to $R_{\max}$. We can describe the OA as a convolution taking place between a complex image and a complex kernel (although this is not the way it was originally described in [11], [12]). The complex image contains the edge-orientation information from the original image. The gradient in the x direction is encoded in the real part of the image and the gradient in the y direction is encoded in the imaginary part. The OA kernel is defined as

$$O_{\mathrm{OA}}(x,y)=\begin{cases} \frac{x-jy}{\sqrt{x^2+y^2}}, & \text{if } R_{\min}^2 < x^2+y^2 < R_{\max}^2 \\ 0, & \text{otherwise.} \end{cases}$$

The center estimate is obtained by finding that pixel with the largest absolute real part in the convolution image. It is not possible to directly obtain a radius estimate using the OA.

IV. Maximum-Likelihood Estimation via Convolution

In this section, we provide a translation between the statistical approach and the image-processing approach. Here, the measurements of Chan's circular functional model are represented as delta functions in what we call an "ideal image." It is then possible to describe maximum-likelihood estimation through a convolution procedure on the image.

A. Ideal Images

We define an *ideal image* of our noisy circular points as one which is unbounded and which is continuous-valued in intensity and in spatial coordinates. Under these conditions, we can make a connection between statistical estimators and image-based estimators by considering the data points as two-dimensional (2-D) delta functions, that is, we can consider the image as a function $f(x,y)$, where

$$f(x,y)=\sum_{i=1}^{N}\delta(x-x_i,y-y_i). \tag{19}$$

If we define a 2-D kernel function

$$g(x,y)=\sqrt{x^2+y^2}$$

then

$$f(x,y)*g^0(x,y)=N \tag{20}$$

$$f(x,y)*g(x,y)=\sum_{i=1}^{N}g(x-x_i,y-y_i)=\sum_{i=1}^{N}r_i \tag{21}$$

$$f(x,y)*g^2(x,y)=\sum_{i=1}^{N}g^2(x-x_i,y-y_i)=\sum_{i=1}^{N}r_i^2. \tag{22}$$

It follows that (10) can be expressed in terms of convolution as follows:

$$F_{\mathrm{ML}}(x,y) = f(x,y) * g^2(x,y) - \frac{(f(x,y) * g(x,y))^2}{f(x,y) * g^0(x,y)}. \quad (23)$$

That is, (23) is an exact interpretation of (10). The MLE is therefore shown to be equivalent to minimizing the intensity of an image obtained through convolution, i.e.,

$$\hat{\mathbf{c}}_{\mathrm{ML}} = \arg\min_{(x,y)} F_{\mathrm{ML}}(x,y)$$

provided a minimum exists.

B. Digital Images

For digital images, the assumptions in Section IV-A do not hold. Digital images have a finite resolution and are only of a certain size. As a result, our model is not entirely accurate, but it can still be applied to good effect. If we have a digital image $f[x,y]$ and a conic kernel $g[x,y]$ (where the square brackets $[\cdot]$ denote the discretised version of the image in (19)) then we can still implement the following equation:

$$F_{\mathrm{ML}} = f[x,y] * g^2[x,y] - \frac{(f[x,y] * g[x,y])^2}{f[x,y] * g^0[x,y]}. \quad (24)$$

Equation (24) describes the computation of a 2-D intensity image, the minimum of which will be the coarse center estimate. Subpixel accuracy can be obtained; this will be discussed in Section VI. By implementing (24) first, we can be more confident that numerical methods will find the globally ML center estimate. We can then use (8) to obtain the radius estimate, $\hat{r}_{\mathrm{ML}}$. In Section VII, we will show that we can achieve subpixel accuracy on synthetic and real digital images.

C. DKE Via Convolution

It is also possible to express the DKE [24] as a convolution equation under the assumptions in Section IV-A. Looking at (13), we can say that

$$\begin{aligned} F_{\mathrm{DK}}(x,y) &= f(x,y) * h^2(x,y) - \frac{1}{N}(f(x,y) * h(x,y))^2 \\ &= f(x,y) * h^2(x,y) - \frac{(f(x,y) * h(x,y))^2}{f(x,y) * h^0(x,y)} \quad (25) \end{aligned}$$

where $h(x,y) = g^2(x,y)$. This can be interpreted as a 2-D intensity image, the minimum of which is the center estimate. The adaptation to digital images follows the same template as for the MLE described in Section IV-B.

V. Approximate MLE

Consider the function

$$\Theta(x,y) = e^{jk\sqrt{x^2+y^2}} \quad (26)$$

where k is some constant. This is what we call a complex phase-coded kernel (PCK) that uses phase to code for radius and can be regarded as another member of a class of kernels which Atherton and Kerbyson call "PCA." When this kernel is convolved with an ideal image, a complex output results whose magnitude can be interpreted as an intensity image where the coordinate of the maximum is the circle-center estimate.

We now define a new objective function F_{AML} by taking the squared magnitude of the convolution of (19) and (26), i.e.,

$$\begin{aligned} F_{\mathrm{AML}} &= |f(c_1,c_2) * \Theta(c_1,c_2)|^2 \quad (27) \\ &= \left(\sum_{i=1}^{N} \cos(k[r+\Delta r_i])\right)^2 \\ &\quad + \left(\sum_{i=1}^{N} \sin(k[r+\Delta r_i])\right)^2 \quad (28) \end{aligned}$$

where r_i was defined in (9) and

$$\Delta r_i = r_i - r = \|\mathbf{p}_i - \mathbf{c}\|_2 - r.$$

The Taylor-series approximation of the cosine and sine terms in (28) is

$$\begin{aligned} \cos(k[r+\Delta r_i]) &= \cos(\mathrm{kr}) - (k\Delta r_i)\sin(\mathrm{kr}) \\ &\quad - \frac{(k\Delta r_i)^2}{2}\cos(\mathrm{kr}) + O\left(\|\Delta r_i\|_2^3\right) \\ \sin(k[r+\Delta r_i]) &= \sin(\mathrm{kr}) + (k\Delta r_i)\cos(\mathrm{kr}) \\ &\quad - \frac{(k\Delta r_i)^2}{2}\sin(\mathrm{kr}) + O\left(\|\Delta r_i\|_2^3\right). \quad (29) \end{aligned}$$

Substituting (29) into (28) and simplifying, it is possible to show that the objective function (27) becomes

$$\begin{aligned} &F_{\mathrm{AML}} \\ &= \left[N\cos(kr) - \sin(kr)\sum_{i=1}^{N} k\Delta r_i \right. \\ &\quad \left. - \frac{\cos(kr)}{2}\sum_{i=1}^{N}(k\Delta r_i)^2\right]^2 \\ &\quad + \left[N\sin(kr) + \cos(kr)\sum_{i=1}^{N} k\Delta r_i \right. \\ &\quad \left. - \frac{\sin(kr)}{2}\sum_{i=1}^{N}(k\Delta r_i)^2\right]^2 \\ &\quad + O\left(\|\Delta r_i\|_2^3\right) \\ &= N^2 - N\sum_{i=1}^{N}(k\Delta r_i)^2 + \left(\sum_{i=1}^{N} k\Delta r_i\right)^2 + O\left(\|\Delta r_i\|_2^3\right) \\ &= N^2 - Nk^2\sum_{i=1}^{N}\|\mathbf{p}_i - \mathbf{c}\|_2^2 + \left\{\sum_{i=1}^{N} k\|\mathbf{p}_i - \mathbf{c}\|_2\right\}^2 \\ &\quad + O\left(\|\Delta r_i\|_2^3\right) \\ &= N^2 - Nk^2\sum_{i=1}^{N} r_i^2 + k^2\left\{\sum_{i=1}^{N} r_i\right\}^2 + O\left(\|\Delta r_i\|_2^3\right). \quad (30) \end{aligned}$$

The expression in (30) is a close approximation to the expression in (10), i.e., the log-likelihood, but with a constant scaling

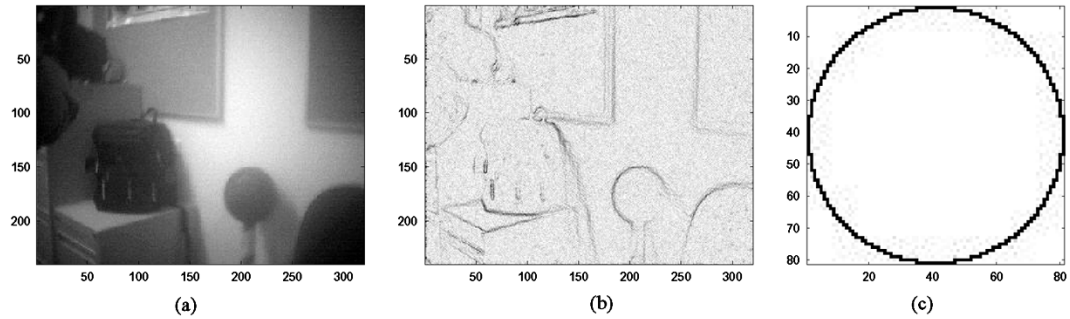

Fig. 3. Image and kernel. (a) Original 320 × 240 image. (b) Negative of edge-magnitude image. (c) 81 × 81 kernel (negative).

and offset factors. Therefore, we have demonstrated an approximate relationship between the PCK and the MLE. The AMLE is, therefore, computed by maximizing the magnitude of a complex image obtained through convolution with an ideal image.

We propose that the PCK could be applied to digital images to implement the AMLE, in the same way that was described for the MLE in Section IV-B. An immediate computational advantage is that the AMLE requires the use of only a single complex convolution rather than three real convolutions for the MLE. The size of the circle is then represented by the phase of the complex convolution at the point where it attains its maximum magnitude.

Furthermore, we expect that another advantage of the AMLE over the MLE when applied to digital images will be a certain amount of robustness to "interferers"— other points, features, or objects in the image other than the circle itself. This is because phase is used to code for radius (26): Circle points are summed in phase, while noncircle points tend to be summed out of phase.

In practice, a disadvantage of the PCK as we have defined it above (and which applies equally to the MLE, and indeed to our statistical model) is that there is no upper bound for the radius. Thus, there is a question as to how large the PCK should be made. A practical approach would then appear to be to make the PCK just large enough to encompass the largest radius which we could expect to encounter in an image. The kernel size would of course depend on the particular application. However, would limiting the kernel size affect the operation of the algorithm? Fortunately, for the PCK, the answer is no, but we cannot do the same for the MLE-via-convolution technique without adversely affecting its performance. This is because the AMLE technique seeks a maximum in the convolution image, whereas the MLE technique seeks a minimum. To see how the MLE would be adversely affected by limiting the size of the kernel, consider a situation in which there is a pixel in the convolution image, far from the true center, for which there is only one pixel with nonzero intensity in the original image within the maximum prescribed radius. From consideration of (24), it can be seen that, in the convolution image, the intensity must be zero at that point and therefore an absolute minimum. This cannot happen with a truncated PCK, and thus the ability to specify a maximum radius in the PCK can be counted a practical advantage over the MLE-via-convolution technique.

Indeed, we can also specify a minimum radius using the PCK, by setting the kernel to zero within this radius. In this case, the PCK, with proper choice of the parameter k, becomes analogous to the PCA, apart from a phase offset, cf. (14) and (26).

VI. Computational Considerations

A. Processor and Memory Utilization

Here, we consider the computation time and memory usage of image-processing algorithms for circle detection and parameter estimation. Our aim here is to compare the CHT with the other convolution-based approaches, especially the AMLE/PCK and the PCA, to obtain coarse center estimates (i.e., to within a pixel).

First, we compare the memory requirements. If the range of possible radii is Δr, and the range in the possible x coordinates of the center is Δa and in the y coordinates Δb, then the memory requirement for the CHT is proportional to the product of all three for the accumulator space. By contrast, the PCK-based approaches (by which we mean the implementation of the AMLE through the PCK as well as the PCA) require a kernel of size proportional to $R_{\max}^2$ and a convolution image of size proportional to $\Delta a \Delta b$. Hence, if the maximum possible radius is small with respect to image size then the PCK-based approaches can require significantly less memory.

As to the computational requirements, both the CHT and the PCK-based approaches depend on convolution. The PCK and PCA require only complex convolution, whereas the CHT requires a number of convolutions proportional to Δr. Hence, except for very small values of Δr (say one or two), the PCK-based approaches will require less computation.

As is well known [26], a "brute force" implementation of convolution for either the CHT or the PCK-based approaches requires a computation time proportional to the product of the sizes of the image and the kernel. However, we can make use of the fast Fourier transform (FFT) to perform convolution very quickly. When the size (total number of pixels) of the image and kernel are the same, say M, convolution can be performed in $O(M \log M)$ arithmetic operations. When the sizes of the image and the kernel are significantly different, computational savings can be achieved through the "overlap-add" or "overlap-save" algorithms. When the size of the kernel is much smaller than the size of the image, convolution will not be significantly faster in the frequency domain. In fact, computation in the frequency domain may be slower for very small kernel sizes.

As an example, consider the 320 × 240 image in Fig. 3(b) and the 81 × 81 kernel in Fig. 3(c). We used the Matlab function `conv2` to perform the brute-force convolution of the edge-magnitude image with the kernel and compared that to the FFT technique. The timings are given in Table I. The FFT technique is almost nine times faster. We note that we used a 2.40-GHz Intel

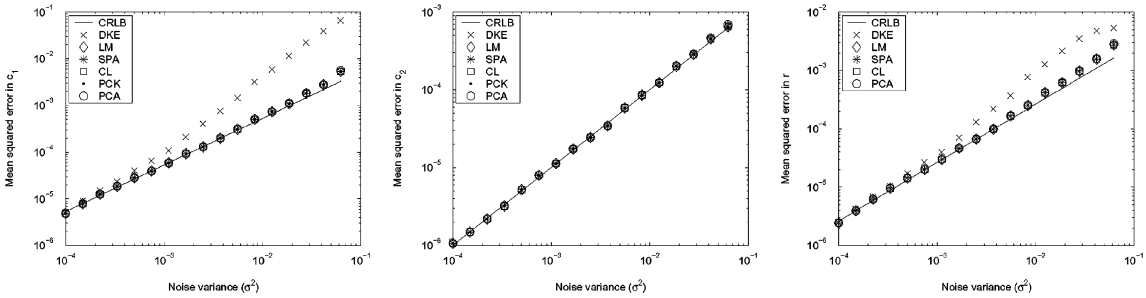

Fig. 4. Simulations results for varying σ for an arc length of 180°.

TABLE I
TIMINGS USING MATLAB'S TIC AND TOC FUNCTIONS

Convolution method	Time (sec)
MATLAB's `conv2` function	1.472
FFT technique	0.168

Xeon CPU with 1.00 GB of RAM, running Microsoft Windows Server 2003 and the Matlab version was 6.5.0.180913a.

B. Achieving Subpixel Center Accuracy

In Section IV-B, we showed that implementing (24) on its own will provide a center estimate to within one pixel. In order to achieve subpixel accuracy with the AMLE, we must treat this coarse estimate as a starting place to numerical gradient-descent (or -ascent) techniques. For the PCK (without radius constraints), we optimize

$$F_{\mathrm{AML}}(c_1, c_2) = \left| \sum_{x,y} f[x,y] e^{jkr(x,y)} \right| \tag{31}$$

where $f[x,y]$ are the intensity values in the edge-magnitude image at pixel (x,y). For the PCA (or the PCK with radius constraints), since we can specify $R_{\min}$ and $R_{\max}$, we can further constrain (x,y) so that

$$F_{\mathrm{PCA}}(c_1, c_2) = \left| \sum_{R_{\min} < r(x,y) < R_{\max}} f[x,y] e^{j\gamma(x,y)} \right|. \tag{32}$$

Equations (31) and (32) can both be optimized using a numerical technique, for instance, the Levenberg–Marquardt (LM) algorithm.

This technique for obtaining subpixel accuracy can be similarly extended to the MLE on digital images.

VII. RESULTS AND SIMULATIONS

Our aim in this section is to show that the AMLE has the "best of both worlds." In a statistical setting, we show that the AMLE does as well as any of the established estimators. In an image-processing setting, we show that the AMLE, via convolution using the PCK or PCA, can be computed quickly and is robust to interference from noncircular objects.

A. Chan's Circular Functional Model

In order to demonstrate the performance of the AMLE relative to other estimators in a statistical setting, two sets of simulations were performed. In the first set of simulations, N was held constant and σ allowed to vary, and *vice versa* in the second set. In both sets, the results were obtained by Monte Carlo analysis.

In the first set of simulations, for each value of σ, the AMLE (28) was evaluated over 1000 independent trials. In each trial, the radius was set to 1 and 200 noisy points $(N = 200)$ were generated in equal angular increments around a half circle to obtain estimates for the center of the circle $\hat{\mathbf{c}}$ and radius $\hat{r}$. This was used to generate mean-square error (MSE) values. The standard deviation, σ, of the noise was varied from 10^{-2} to 0.25 in equal geometric increments. The AMLE was compared against the DKE and several methods for numerically evaluating the MLE: direct application of the LM algorithm on the log-likelihood function (here abbreviated as LM), the Späth algorithm (SPA) and the CL algorithm. The DKE was used to initialize all other estimators. For the AMLE implementation through the PCK, the parameter k in (26) was set to 1.

The MSE values in $\hat{\mathbf{c}}$ and $\hat{r}$ for the AMLE, DKE, SPA, LM and CL methods are plotted against their corresponding CRLBs (4) for the same level of noise σ in Fig. 4 on a logarithmic scale. It can be seen that as the noise level σ approaches zero, the estimators $\hat{\mathbf{c}}$ and $\hat{r}$ approach the CRLB. As noise variance increases, the AMLE, SPA, MLE, and CL methods deviate from the CRLB after the DKE. The poor performance of the DKE is not surprising. Its shortcomings at high noise levels are well documented [17], [24]. The results for the AMLE in Fig. 4 are good as they show that the AMLE's performance is very similar to that of the numerical ML methods. As there is no radius estimate with the PCK because there is no upper bound for the radius (see the discussion at the end of Section V), the MSE in $\hat{r}$ is not plotted for the PCK in Fig. 4(c).

In the second set of simulations, σ was fixed and N was varied. For each value of N, the AMLE, DKE, SPA, LM, and CL methods were evaluated over 1 000 trials. In each trial, σ was set to 0.1 and the number of points were varied from $N = 3$ to $N = 100$ and they were generated in equal increments around the right half of a circle's circumference to obtain estimates for the center of the circle $\hat{\mathbf{c}}$ and radius $\hat{r}$. This was used to generate MSE values.

The MSE values in $\hat{\mathbf{c}}$ and $\hat{r}$ for all five methods are plotted against the corresponding CRLB for each value of N in Fig. 5 on a logarithmic scale. Observe that the CRLB for $\hat{c}_2$ is lower

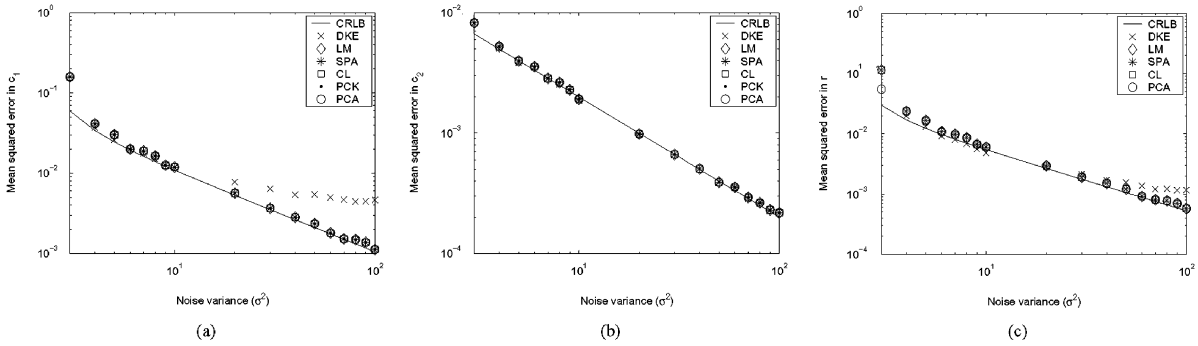

Fig. 5. Simulations results for varying N for an arc length of 180°.

than that for $\hat{c}_1$. This is because the arc over which the circumferential points were arranged was a right half circle. For this arc, more localization is possible in $\hat{c}_2$ than in $\hat{c}_1$.

Apart from the DKE, all other methods appear to follow the CRLB as N increases. The results for the DKE are not surprising because the DKE is not asymptotically efficient [17], [24]. Again, the AMLEs performance is very similar to that of the ML methods and the results suggest that it may be asymptotically efficient. Again, we note that there is no radius estimate with the PCK and so the MSE in $\hat{r}$ is not plotted for the PCK in Fig. 5(c).

B. Noisy Circles in Synthetic Digital Images

Having examined performance of the AMLE relative to other methods in a standard statistical setting, we now turn our attention to its performance in synthetic and real digital images. For the first evaluation of the AMLE in digital images, synthetic digital images of circles were created. A set of simulations was conducted to determine the MSE performance of the AMLE technique relative to the DKE and numerical MLE techniques. MSE performance was again evaluated using Monte Carlo analysis. In each trial, a 128×128 synthetic image was created with 200 $(N = 200)$ noisy points around a full circle with a radius of 32. The center of the circle was varied randomly from trial to trial so that each center coordinate was uniformly distributed between 63.5 and 64.5. In forming the digital image, the positions of the noisy points on the circumference were, naturally, quantised to the nearest pixel. Where more than one noisy point was quantised to the same pixel, that pixel's intensity was incremented appropriately. The standard deviation, σ, of the noise was varied from 10^{-2} to 1. One thousand trials were conducted (i.e., images were generated) for each value of σ.

For each trial image, the AMLE, DKE, and numerical MLEs were computed. The estimates were each computed in two steps. First, convolution with an appropriate kernel was performed as described in Sections IV and V. The convolution yields a "coarse" estimate to the nearest pixel. Subpixel accuracy is then obtained using the iterative numerical techniques discussed in Section VI-B. The astute reader will observe that there is no reason to take this two-step approach for calculating the DKE, since this estimate can be computed in closed form. Indeed, it is the closed-form version of the DKE that was used by the authors in conducting these simulations.

In assessing the MSE results, it is clear that the CRLB for Chan's circular functional model is no longer directly applicable. How then can we know whether an estimator is performing as well as can be hoped? We offer no definitive answer and the literature is sparse (Vosselman and Haralick [27] is the only work on this topic of which the authors are aware, and their results are not directly applicable in this scenario). However, as a guide to the level of MSE that we might achieve, we offer the following approximation, which appears to serve well in practice (as we shall see in Fig. 6). This approximation uses the CRLB of Chan's circular functional model as its starting point, but regards the quantization process in the formation of the synthetic digital image as an additional and independent noise source. Since the centers have been chosen randomly in each trial with respect to the quantization (pixel) boundaries, and N is not too great, this assumption is quite good. The quantization process is modeled as having zero mean and variance $1/12$. Thus, allowing for the additional variance of the quantization, the CRLB of (4) of Chan's functional model may be adapted so that the variances

$$\sigma^2_{\hat{c}_1} = \frac{\frac{1}{12} + 2\sigma^2}{N - \Psi}, \quad \sigma^2_{\hat{c}_2} = \frac{\frac{1}{12} + 2\sigma^2}{N - \Xi} \quad \text{and} \quad \sigma^2_{\hat{r}} = \frac{\frac{1}{12} + \sigma^2}{N - \Omega} \tag{33}$$

provide a guide to the MSEs that might be expected from "good" circle estimators in practice. Observe that, as σ goes to zero, the MSE of the estimates will not also go to zero but will plateau due to the quantization noise.

The MSE values are plotted in Fig. 6 on a logarithmic scale. Because the noisy points were spaced around a full circle, the results for $\hat{c}_2$ have been ommitted as they are not significantly different to those of $\hat{c}_1$. It can be seen that the estimators $\hat{c}_1$ and $\hat{r}$ conform closely to the variance guide provided by (33). For the PCK, there is no radius estimate (that is, not an unambiguous one) as there is no upper bound for the radius (see the discussion at the end of Section V) and so the MSE in $\hat{r}$ is not plotted for the PCK in Fig. 6(b).

In the simulation results presented so far, we have only been able to demonstrate that the AMLE appears to perform *no worse* than estimators that have been established for some considerable time in the literature. However, an important advantage of the AMLE over other methods lies in the fact that, as well as being no worse than traditional estimators in statistical settings and

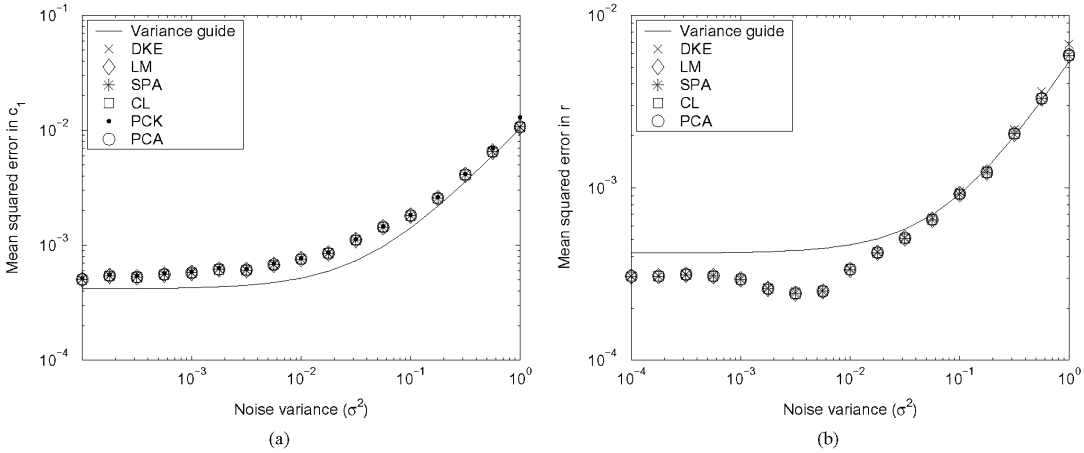

Fig. 6. Simulation results for varying σ for an arc length of 360°.

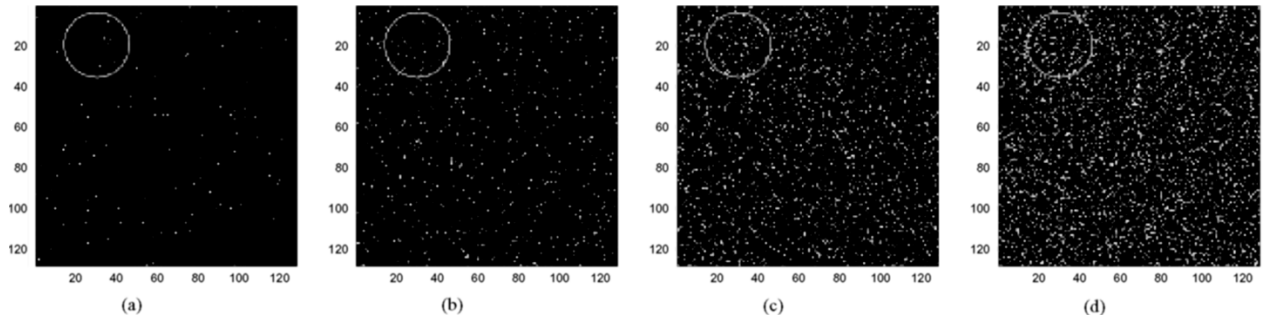

Fig. 7. Synthetic digital images with varying amounts of salt and pepper noise added.

in controlled synthetic digital image experiments, the AMLE is robust to the sorts of interferences that are encountered in real digital images. A second advantage is that the AMLE can be computed very quickly. Another experiment on synthetic digital images was performed which begins to demonstrate these advantages.

In this second set of simulations on synthetic digital images, 128×128 images were generated in which a circle was drawn with center (arbitrarily) set to (30.34, 19.51) and radius 16. Although no noise was added to points around the circumference of the circle, varying amounts of salt-and-pepper noise were added throughout the image. This is depicted in Fig. 7. Clearly, this is now a significant departure from Chan's circular functional model.

For each of these images, the AMLE was compared with the DKE and the MLE (LM algorithm). In each case, the two-step approach of convolution followed by subpixel optimization was performed, except, as noted above, for the DKE, which can be computed directly in closed form. The amount of CPU time required to compute the "coarse" and "fine" estimates was recorded (for the DKE, only the "fine" estimate computation time is applicable).

As discussed in Section V, an advantage of the implementation of the AMLE through convolution is that the PCK can be trimmed if prior knowledge on the range of possible radii is at hand. In such cases, the coarse estimation procedure can be conducted using the PCA. In conducting this set of simulations, two variants of the AMLE kernel were used. One was the PCK, which was made large enough to take in the entire image (thus simulating no prior knowledge of the range of possible radii). The other was the PCA, in which the kernel was trimmed to take in only radii between 8 and 24.

In addition to the statistical methods, the CHT was also used for comparison. Integer search radii in the range from 8 to 24 were used, as for the PCA. No optimization step was performed to achieve subpixel accuracy from the CHT.

The results, timings (coarse and fine) and errors are summarized in Table II. There are several observations to be made. First, we notice that the MLE and DKE grossly misestimate the circle center and radius, regardless of the level of applied salt-and-pepper noise. This is because the "salt" noise seduces the center estimate away the true circle center in order to attain a global minimum in the empirical variance of the radius to each point (or squared radius in the case of the DKE). The PCK implementation of the AMLE also exhibits this defect, although only at the two highest levels of salt-and-pepper noise. We again note that there is no radius estimate with PCK for reasons already discussed. However, both the CHT and the PCA exhibit good and stable estimates of the circle center and radius at all noise levels. For high levels of noise, it is not clear if there is any benefit in the subpixel optimization performed for the PCA.

A clear benefit of the PCA over the CHT is the amount of CPU time required to compute the estimates. To compute an

TABLE II
RESULTS, TIMINGS, AND ERRORS FOR THE IMAGES IN FIG. 7

	CHT			PCA			PCK			MLE			DKE		
Image	$\hat{c}_1$	$\hat{c}_2$	$\hat{r}$	$\hat{c}_1$	$\hat{c}_2$	$\hat{r}$	$\hat{c}_1$	$\hat{c}_2$	$\hat{r}$	$\hat{c}_1$	$\hat{c}_2$	$\hat{r}$	$\hat{c}_1$	$\hat{c}_2$	$\hat{r}$
img_1	30	20	16	30.20	19.45	16.11	30.57	19.43	—	56.57	61.88	49.71	57.93	58.93	51.28
img_2	30	20	16	30.06	19.71	16.45	29.99	19.04	—	65.54	63.49	50.44	64.59	64.00	53.39
img_3	30	20	16	30.16	19.77	16.53	87.27	62.87	—	62.87	64.50	49.15	63.31	64.22	52.37
img_4	30	20	16	29.87	20.59	16.91	8.16	83.69	—	63.55	64.30	48.80	64.15	64.15	52.05

	CHT timings (sec)		PCA timings (sec)		PCK timings (sec)		MLE timings (sec)		DKE timings (sec)	
Image	coarse	fine	coarse	fine	coarse	fine	coarse	fine	coarse	fine
img_1	1.768	—	0.124	0.404	0.434	0.078	1.287	0.186	—	0.031
img_2	1.743	—	0.132	0.351	0.425	0.059	1.230	0.132	—	0.029
img_3	1.753	—	0.122	0.351	0.442	0.107	1.341	0.153	—	0.031
img_4	1.436	—	0.115	0.488	0.346	0.128	1.077	0.129	—	0.031

	CHT errors in			PCA errors in			PCK errors in			MLE errors in			DKE errors in		
Image	c_1	c_2	r	c_1	c_2	r	c_1	c_2	r	c_1	c_2	r	c_1	c_2	r
img_1	-0.34	0.49	0	-0.14	-0.06	0.11	0.23	-0.08	—	26.23	42.37	33.71	27.59	39.42	35.28
img_2	-0.34	0.49	0	-0.28	0.2	0.45	-0.35	-0.47	—	35.20	43.98	34.44	34.25	44.49	37.39
img_3	-0.34	0.49	0	-0.18	0.26	0.53	56.93	43.36	—	32.53	44.99	33.15	32.97	44.71	36.37
img_4	-0.34	0.49	0	-0.47	1.08	0.91	-22.18	64.18	—	33.21	44.79	32.80	33.81	44.64	36.05

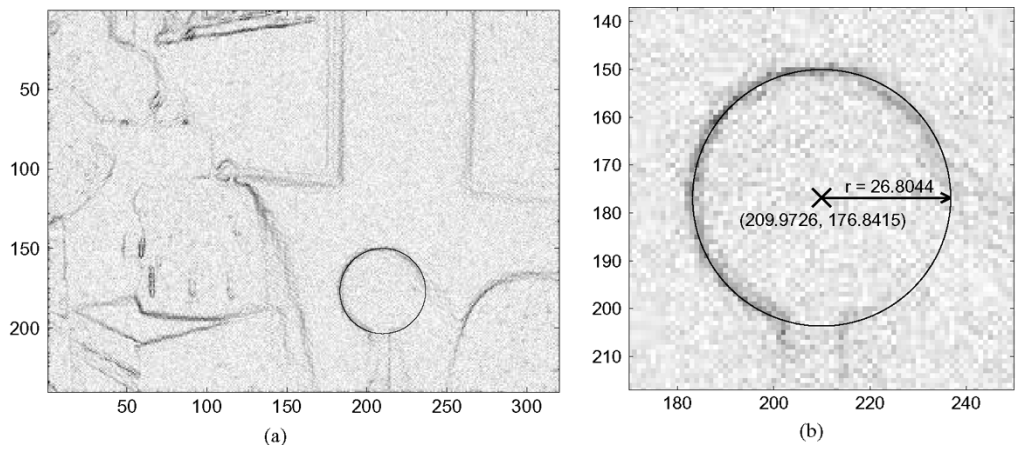

Fig. 8. Performance of the PCA on a real digital image. (a) Negative of edge-magnitude image with circle estimates overlaid. (b) A close-up of Fig. 8(a).

equivalent (coarse) estimate, the PCA requires less than a tenth of the computation time of the CHT.

C. Photographic Digital Images

To conclude this section, we turn to a couple of examples on real, photographic digital images, to further illustrate the AMLE's robustness and accuracy.

Consider again the image with the basketball in Fig. 3 which was taken with a common digital web camera. The image is not of a particularly high quality and when we look at the edge-magnitude image (or, rather, its negative) in Fig. 3(b), we see that there are plenty of edge points which do not belong to the circle. With the minimum and maximum radii of the PCA kernel set to $R_{\min} = 20$ and $R_{\max} = 30$, respectively, it was convolved with the edge-magnitude image to obtain a complex image result. The magnitude of this complex image had a maximum at position (210, 177), this being the "coarse" center estimate. The phase of the complex image at this position was then substituted into (15) in order to solve for the radius. The resulting radius estimate was $\hat{r} = 26.8044$. After subpixel optimization, as discussed in Section VI-B, the center estimate was refined to (209.7926, 176.8415). This circle is overlayed on top of the edge magnitude image in Fig. 8. It can be seen that this is visually a good fit.

As a last example, we compare the AMLE, as implemented by the PCA, and the orientation annulus (OA). Although the OA makes use of edge orientation information which is ignored by the AMLE (in favor of edge magnitude information alone), we demonstrate that this information is not always used to good effect, and can in fact be detrimental. Fig. 9(a), shows a case where the orientation annulus produces a poor result. It shows a tennis ball against a checkered black-and-white background. Part of the circumference of the tennis ball in the image is set against a black background, and part against a white background. The

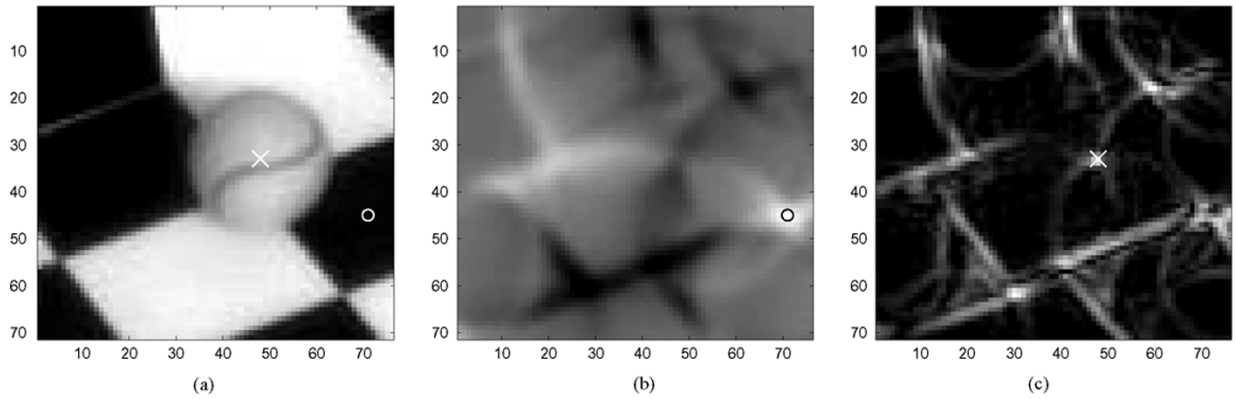

Fig. 9. Performance of the OA compared to that of the PCA. (a), (b) OA applied on the image in Fig. 9(a). (c) Magnitude of the PCA applied on the image in Fig. 9(a)

edge gradient around the circumference is therefore neither directed uniformly inwards nor uniformly outwards. Hence, convolution with the OA kernel fails to produce a prominent peak in the absolute real part. In contrast, the PCA kernel produces a strong peak in the close vicinity of its true location and, additionally, a radius estimate of 15.3534 can be directly calculated. For both the OA and PCA kernels, values of $R_{\min} = 13$ and $R_{\max} = 17$ were used.

VIII. Conclusion

In this paper, we have presented a unified view of estimators for circle center and radius. We tie together the statistical viewpoint, in which a circle is represented as a list of noisy measurements around the circumference, and the image-processing viewpoint, in which the circle is represented by high-intensity pixels near the circumference. The maximum-likelihood estimator in Chan's circular functional model [13] is shown to be represented in an image-processing context by convolution with appropriate kernels. The widely-used DKE [5], [18] can be similarly represented by convolution.

Further, we show that an AMLE can be developed using a phase-coded kernel. The AMLE can be made almost identical in form to the popular PCA [11], [12] when applied to images.

Through simulation studies, we examine the properties of the MLE and the AMLE both from a statistical viewpoint and an image-processing viewpoint. We find that the AMLE has virtually identical properties to the MLE. The AMLE appears to be statistically efficient whenever the MLE is. When applied to digital images, the AMLE has several advantages over traditional image-processing methods such as the CHT [9], [10] and even the MLE. We demonstrate that it can give excellent subpixel accuracy, can be computed quickly (by virtue of the implementation of convolution using the FFT), and, when prior information is available to adequately constrain the range of radii, is highly robust to interference from extraneous edges contributed by noncircular objects.

The structure of the AMLE and PCA and their robustness to interference raises the question of whether these estimators might also be used as detectors. Empirically, the answer is that they appear to make excellent circle detectors. However, in future research, the authors will try to quantify their performance in this regard. Also, although it appears that the AMLE is asymptotically efficient, this has not yet been proved. This is something the authors intend to pursue.

References

[1] U. M. Landau, "Esimation of a circular arc center and its radius," *Comput. Vis. Graph. Image Process.*, vol. 38, pp. 317–326, Jun. 1986.
[2] J. F. Crawford, "A noniterative method for fitting circular arcs to measured points," *Nucl. Instrum. Meth. Phys. Res.*, vol. 211, pp. 223–225, 1983.
[3] V. Karimäki, "Effective circle fitting for particle trajectories," *Nucl. Instrum. Meth. Phys. Res. A*, vol. 305, pp. 187–191, 1991.
[4] A. Thom, "A statistical examination of the megalithic sites in Britain," *J. Roy. Stat. Soc. Ser. A*, vol. 118, pp. 275–295, Mar. 1955.
[5] I. Kåsa, "A circle fitting procedure and its error analysis," *IEEE Trans. Instrum. Meas.*, vol. 25, no. 1, pp. 8–14, Mar. 1976.
[6] G. Coath and P. Musumeci, "Adaptive arc fitting for ball detection in robocup," in *Proc. APRS Workshop on Digital Image Computing*, Brisbane, Australia, Feb. 2003, pp. 63–68.
[7] H. Späth, "Least-square fitting by cirles," *Computing*, vol. 57, pp. 179–185, 1996.
[8] N. Chernov and C. Lesort, "Least squares fitting of circles and lines," *J. Math. Imag. Vis.*, to be published.
[9] R. O. Duda and P. E. Hart, "Use of the hough transform to detect lines and curves in pictures," *Commun. ACM*, vol. 15, pp. 11–15, 1972.
[10] E. Trucco and A. Verri, *Introductory Techniques for 3D Computer Vision*. Englewood Cliffs, NJ: Prentice-Hall, 1998.
[11] T. J. Atherton and D. J. Kerbyson, "Size invariant circle detection," *Image Vis. Comput.*, vol. 17, pp. 795–803, Aug. 1999.
[12] D. J. Kerbyson and T. J. Atherton, "Circle detection using hough transform filters," *Image Process. Appl.*, pp. 370–374, 1995.
[13] N. N. Chan, "On circular functional relationships," *J. Roy. Statist. Soc. Ser. B*, vol. 27, pp. 45–56, Apr. 1965.
[14] S. M. Robinson, "Fitting spheres by the method of least squares," *Commun. ACM*, vol. 4, p. 491, 1961.
[15] Y. T. Chan and S. M. Thomas, "Cramér–Rao lower bound for estimation of a circular arc center and its radius," *Graph. Models Image Process.*, vol. 57, pp. 527–532, Nov. 1995.
[16] K. Kanatani, "Cramér–Rao lower bounds for curve fitting," *Graph. Models Image Process.*, vol. 60, pp. 93–99, 1998.
[17] M. Berman and D. Culpin, "The statistical behavior of some least squares estimators of the centre and radius of a circle," *J. Roy. Stat. Soc. Ser. B*, vol. 48, pp. 183–196, Oct. 1986.
[18] P. Delogne, "Computer optimization of Deschamps' method and error cancellation in reflectometry," in *Proc. IMEKO-Symp. Microwave Measurements*, Budapest, Hungary, 1972, pp. 117–123.
[19] S. M. Thomas and Y. T. Chan, "A simple approach to the estimation of circular arc center and its radius," *Comput. Vis. Graph. Image Process.*, vol. 45, pp. 362–370, Aug. 1989.
[20] I. D. Coope, "Circle fitting by linear and nonlinear least squares," *J. Optim. Theory Appl.*, vol. 76, pp. 381–388, Feb. 1993.
[21] L. Moura and R. Kitney, "A direct method for least-squares circle fitting," *Comput. Phys. Commun.*, vol. 64, pp. 57–63, 1991.
[22] D. Umback and K. N. Jones, "A few methods for fitting circles to data," *IEEE Trans. Instrum. Meas.*, vol. 52, no. 6, pp. 1881–1885, Dec. 2003.

[23] E. E. Zelniker and I. V. L. Clarkson, "A statistical analysis of least squares circle-centre estimation," in *Proc. IEEE Int. Symp. Signal Process. Inform. Tech.*, Darmstadt, Germany, Dec. 2003.
[24] ——, "A statistical analysis of the Delogne–Kåsa method for fitting circles," *Digital Signal Process.*, to be published.
[25] H. L. Van Trees, *Detection, Estimation and Modulation Theory*. New York: Wiley, 1968.
[26] A. V. Oppenheim and R. W. Schafer, *Discrete-Time Signal Processing*. Englewood Cliffs, NJ: Prentice-Hall, 1999.
[27] G. Vosselman and R. M. Haralick, "Performance analysis of line and circle fitting in digital images," presented at the Proc. Workshop on Performance Characteristics of Vision Algorithms, Cambridge, MA, Apr. 1996.

Emanuel E. Zelniker (S'03) was born in Beer-Sheva, Israel, in 1979. He received the B.E. degree with first-class honors in electrical engineering from the University of Queensland, Brisbane, Australia, in 2001, and is currently pursuing the Ph.D. degree at the School of Information Technology and Electrical Engineering, University of Queensland.

His areas of research are image analysis, detection, and estimation.

Mr. Zelniker is the recipient of the Commonwealth Scientific and Industrial Research Organization Scholarship.

I. Vaughan L. Clarkson (S'93–M'98–SM'04) was born in Brisbane, Australia, in 1968. He received the B.Sc. degree in mathematics and the B.E. degree with first-class honors in computer systems engineering from the University of Queensland, Brisbane, in 1989 and 1990, respectively, and the Ph.D. degree in systems engineering from the Australian National University, Canberra, in 1997.

Starting in 1988, he joined the Defence Science and Technology Organization, Adelaide, Australia, first as a Cadet, later as a Professional Officer, and, finally, as a Research Scientist. From 1998 to 2000, he was a Lecturer with the University of Melbourne, Melbourne, Australia. Since 2000, he has been a Senior Lecturer in the School of Information Technology and Electrical Engineering, University of Queensland. In 2005, he was a Visiting Professor with the Department of Electrical and Computer Engineering, University of British Columbia, Vancouver, BC, Canada. His research interests include statistical signal processing for communications and defense, image processing, information theory, and lattice theory.